

# Non-invasive monitoring of living cell culture by lensless digital holography imaging

Yunxin Wang (王云新)<sup>1</sup>, Dayong Wang (王大勇)<sup>1\*</sup>, Jie Zhao (赵洁)<sup>1</sup>,  
Yishu Yang (杨怡殊)<sup>2</sup>, Xiangqian Xiao (肖向茜)<sup>2</sup>, and Huakun Cui (崔华坤)<sup>1</sup>

<sup>1</sup>College of Applied Sciences, Beijing University of Technology, Beijing 100124, China

<sup>2</sup>College of Life Science and Biotechnology, Beijing University of Technology, Beijing 100124, China

\*Corresponding author: wdyong@bjut.edu.cn

Received September 16, 2010; accepted November 2, 2010; posted online February 21, 2011

A non-invasive detection method for the status analysis of cell culture is presented based on digital holography technology. Lensless Fourier transform digital holography (LFTDH) configuration is developed for living cell imaging without prestaining. Complex amplitude information is reconstructed by a single inverse fast Fourier transform, and the phase aberration is corrected through the two-step phase subtraction method. The image segmentation is then applied to the automatic evaluation of confluency. Finally, the cervical cancer cell TZMbl is employed for experimental validation, and the results demonstrate that LFTDH imaging with the corresponding image post-processing can provide an automatic and non-invasive approach for monitoring living cell culture.

OCIS codes: 090.0090, 170.0170, 100.0100, 120.0120.

doi: 10.3788/COL20110.030901.

Cell culture technology plays an important role in the development of modern life science and the biomedical discipline. Cells will proliferate exponentially under a suitable environment. However, they will be damaged in the form of necrosis or apoptosis when the culture environment deteriorates<sup>[1,2]</sup>. Therefore, the variation in the number of cells is commonly employed to describe the cell proliferative potential and cell viability. Confluency, as an important parameter for culture status, refers to the density of cells in their growth environment, which helps to determine the proper time for cell passage. Cell density is conventionally determined by the manual counting method with haemocytometer<sup>[3]</sup>, which is relatively tedious and has limited accuracy in view of human factors. Several automatic cell counters have been developed recently, but all of them require the prestaining of cells by chemical reagents such as trypan blue or propidium iodide<sup>[4]</sup>. Because of these issues, many optical methods have been studied to achieve the visual observation of living cells, such as Fourier phase microscopy (FPM)<sup>[5]</sup>, Hilbert phase microscopy (HPM)<sup>[6]</sup>, diffraction phase microscopy (DPM)<sup>[7]</sup>, and digital holographic microscopy (DHM)<sup>[8,9]</sup>. Among these, DHM attracts the most remarkable attention for several advantages. The quantitative amplitude and phase information of the object wavefront can be retrieved from a single digital hologram, which makes real-time detection possible. DHM does not demand the recording of the hologram in the focus image plane of the object. Furthermore, DHM does not require complex scanning configuration since it has a simple setup. Many researchers have engaged in non-invasive cell imaging using DHM. Depeursinge *et al.* detected the physiological parameters of neurons and testate amoebae, using pre-magnification digital holography<sup>[10,11]</sup>. Bemper *et al.* studied the invasion mechanism of living pancreas carcinoma cells and the interaction mechanism of the anticancer drug based on the DHM system<sup>[12]</sup>. Recently, the cell imaging instrument Holomonitor<sup>TM</sup> was

developed by the company Phase Holographic Imaging AB in Sweden, and Mölder *et al.* used this instrument to achieve cell counting measurement<sup>[13]</sup>. However, the robust configuration of DHM and its new applications still require further research.

Several recording approaches can be done to digital holography, such as the off-axis Fresnel holography and the pre-magnification digital holography. However, these methods do not use the spatial bandwidth of the image sensor entirely, and reconstruction algorithms are time consuming due to the need to calculate Fourier transform several times. The larger the view field of the imaging system, the more reliable the detection of the confluency for cell culture will be. Although pre-magnification digital holography exhibits high resolution, the limited view field prevents it from being able to measure cell density. All these problems can be settled effectively by the lensless Fourier transform digital holography (LFTDH). The LFTDH method can fully use the spatial bandwidth of the sensor and the system's setup and reconstruction algorithm are relatively simple, making it suitable for the status evaluation of cell culture. In this letter, the

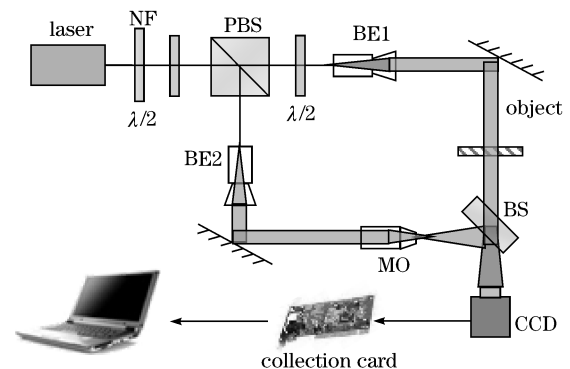


Fig. 1. Schematic diagram of LFTDH configuration. NF: neutral filter. BE: beam expander; MO: microscope objective.

LFTDH configuration is designed for cell imaging without prestaining, and the reconstructed complex amplitude can be obtained from the digital hologram by a single inverse fast Fourier transform. The image analysis technology is then combined for the automatic detection of the status of cell culture. In the experiments, the cervical cancer cell TZMbl, which is a type of adherent cell, is taken as an example. In addition, the phase-contrast image and the level of confluency are given.

The schematic of the experimental setup for the status evaluation of cell culture is illustrated in Fig. 1, which is based on the Mach-Zehnder interferometer. The input laser is divided into two parts by a polarization beam splitter (PBS): one beam goes through the transparent or semi-transparent test sample as the object beam, while the other beam is expanded and filtered to produce a finer reference point source. The object and reference beams are combined at the beam splitter (BS); the interference pattern is recorded by the charge-coupled device (CCD) detector; and the image data are sent to a computer through a collection card. The intensity ratio between the reference and object beams can be adjusted by the combination of  $\lambda/2$  half-wave plate and PBS to improve the image quality of the digital hologram. In the experiments, the laser Verdi-5 with wavelength of 532 nm is used. The CCD has  $4016 \times 2672$  (pixels), with each pixel measuring  $9 \times 9$  ( $\mu\text{m}$ ).

In the LFTDH system, the cross section of the test sample and the reference point source should be located in the same plane<sup>[14]</sup>. According to the Fresnel diffraction integral, the object wave field arriving at the hologram plane can be represented as

$$\begin{aligned} u(x, y) &= \exp\left[j\frac{k}{2z_0}(x^2 + y^2)\right] \iint_{-\infty}^{\infty} o(x_0, y_0) \\ &\exp\left[j\frac{k}{2z_0}(x_0^2 + y_0^2)\right] \exp\left[-j\frac{2\pi}{\lambda z_0}(xx_0 + yy_0)\right] dx_0 dy_0 \\ &= \exp\left[j\frac{k}{2z_0}(x^2 + y^2)\right] F\left\{o(x_0, y_0) \exp\left[j\frac{k}{2z_0}(x_0^2 + y_0^2)\right]\right\}, \end{aligned} \quad (1)$$

where  $k$  is the wave number,  $o(x_0, y_0)$  is the complex amplitude distribution of the object in the object plane,  $z_0$  is the recording distance, and  $F\{\cdot\}$  denotes the Fourier transform operation.

The reference wave field arriving at the hologram plane is expressed as

$$r(x, y) = \exp\left[j\frac{jk}{2z_0}(x^2 + y^2)\right] \exp\left[-j\frac{jk}{z_0}(xx_r + yy_r)\right], \quad (2)$$

where  $(x_r, y_r)$  is the coordinate of the reference point source in the object plane. The hologram in the CCD plane can be expressed by the combination of four terms:

$$\begin{aligned} I(x, y) &= |u(x, y) + r(x, y)|^2 \\ &= |u(x, y)|^2 + |r(x, y)|^2 \\ &\quad + u(x, y)r^*(x, y) + u^*(x, y)r(x, y), \end{aligned} \quad (3)$$

where  $*$  denotes the complex conjugate operator.

The hologram can be delivered to a computer through a collection card, and the reconstructed image can then

be achieved. From Eq. (3), we can see that the reconstructed image has three parts: the zero-order image caused by the first two terms, the original image from the third term, and the virtual image from the fourth term. The three parts can be separated under a reasonable experimental condition. In this letter, only the second part of the reconstructed image is analyzed, and this can be obtained using Eqs. (1) and (2)

$$\begin{aligned} u(x, y)r^*(x, y) &= \exp\left[j\frac{2\pi}{\lambda z_0}(xx_r + yy_r)\right] F\left\{o(x_0, y_0)\right. \\ &\quad \left.\exp\left[j\frac{k}{2z_0}(x_0^2 + y_0^2)\right]\right\}. \end{aligned} \quad (4)$$

Since the first-order linear phase factor can only lead to the shift in the reconstructed image, the reconstruction of the hologram obtained by the LFTDH system can be achieved by one inverse fast Fourier transform. The reconstruction of the complex amplitude distribution is

$$\begin{aligned} U_3(x', y') &= \int \int_{-\infty}^{\infty} u(x, y)r^*(x, y) \\ &\quad \exp\left[j\frac{2\pi}{\lambda z_0}(x'x + y'y)\right] dx dy \\ &= (\lambda z_0)^2 o(x' + x_r, y' + y_r) \exp \\ &\quad \left\{j\frac{k}{2z_0}[(x' + x_r)^2 + (y' + y_r)^2]\right\}. \end{aligned} \quad (5)$$

Therefore, the amplitude reconstruction result is the accurate information of the object at the center  $(-x_r, -y_r)$ , and the sampling interval of the reconstruction of image plane is  $\lambda z_0/N\Delta x$ , where  $N$  and  $\Delta x$  are the pixel number and pixel size of the CCD, respectively. The quadratic phase factor evidently results in the phase aberration, which is closely related to the recording distance and the location of the reference light. However, these parameters are difficult to be measured accurately in experiments. Therefore, we used the two-step phase subtraction method to eliminate phase aberration<sup>[15]</sup>. If we remove the test sample and record another hologram, the reconstructed complex amplitude distribution can then be expressed as

$$\begin{aligned} U'_3(x', y') &= (\lambda z_0)^2 \\ &\quad \exp\left\{j\frac{k}{2z_0}[(x' + x_r)^2 + (y' + y_r)^2]\right\}. \end{aligned} \quad (6)$$

The phase aberration is clearly the same as that of the test sample. Therefore, the phase subtraction between  $U'_3(x', y')$  and  $U_3(x', y')$  can be adopted to eliminate the phase aberration to a great extent. The phase can be obtained by

$$\phi(m, n) = \arctan \frac{\text{Im}[U'_3(x', y')]}{\text{Re}[U'_3(x', y')]} - \arctan \frac{\text{Im}[U_3(x', y')]}{\text{Re}[U_3(x', y')]}, \quad (7)$$

where  $\text{Re}[\cdot]$  and  $\text{Im}[\cdot]$  denote the real and imaginary parts of the complex amplitude, respectively.

When the optical depth of the test sample is greater than the wavelength  $\lambda$ , the phase image will contain  $2\pi$  discontinuities for the principle of the arctan function. The least-squares phase-unwrapping algorithm is applied to acquire accurate phase information<sup>[16]</sup>.

The living cell culture of cervical cancer cell TZMbl

was prepared for the experimental research. For convenience, the living cervical cancer cells were cultured on a glass slide in a petri dish. After the breeding period, the glass slide with the cervical cancer cells was dredged up and covered by a cover glass, as shown in Fig. 2; this was used as the test sample. The hologram of the living cells, which was cut into  $2672 \times 2672$  (pixels), was captured by the LFTDH configuration. The intensity distribution of the hologram was obtained by a single inverse fast Fourier transform, and the section that includes the cell information was intercepted to reduce the computational complexity. Figures 3(a)–(c) show the reconstructed amplitude image of the whole field, part of the real image, and the wrapped phase image of the living cells, respectively. Afterwards, the sample of the living cells was removed; the corresponding reconstructed amplitude image of the whole field, part of the real image, and the wrapped phase image are shown in Figs. 3(d)–(f). The two-step phase subtraction method was then applied to correct the phase aberration, and the unwrapped phase image of the living cells can be acquired, as shown in Fig. 4. In the experiments, the recording distance  $z_0$  was about 89 mm, and the sam-

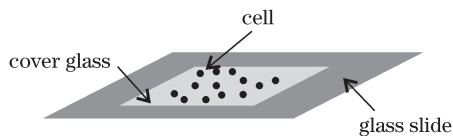


Fig. 2. Schematic diagram for the sample of living cell culture.

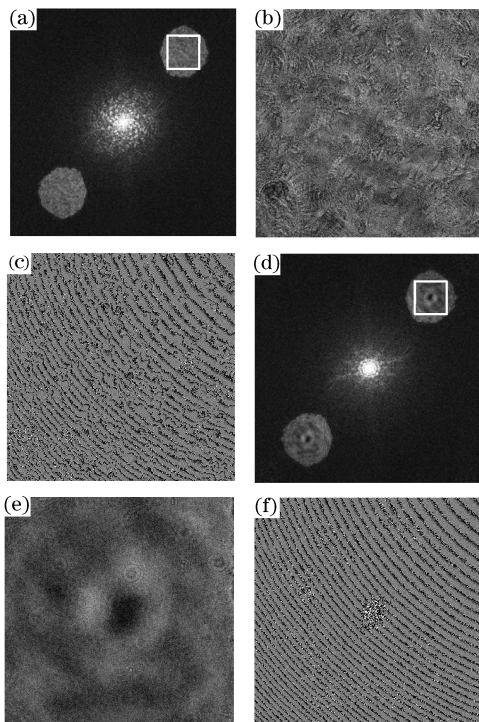


Fig. 3. Experimental results using the cervical cancer cell TZMbl as sample: (a)–(c) with the existence of the object, the reconstructed amplitude image of the whole field, part of the real image in the pane of Fig. 3(a), and the wrapped phase image, respectively; (d)–(f) with the absence of the object, the reconstructed amplitude image of the whole field, part of the real image in the pane of Fig. 3(d), and the wrapped phase image.

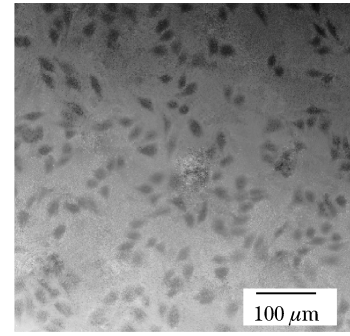


Fig. 4. Unwrapped phase image after phase aberration.

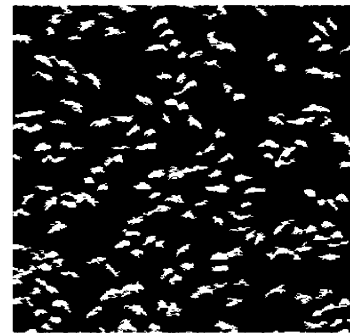


Fig. 5. Segmenting result for the unwrapped phase image in Fig. 4.

pling interval of the reconstruction image plane was  $1.97 \mu\text{m}$ . The distribution of the living cells can be clearly identified, which provides the basic information for the analysis of the cell culture. However, because the culture medium is uneven or part of the residual phase aberration was not removed thoroughly, the gray distribution of the background in the unwrapped phase image was not uniform, which causes the difficulty in calculating the level of confluency. Fortunately, the image processing technology can be combined to greatly reduce the influence of the quality of imaging.

Since living cell is quasi-transparent, its morphology can hardly be distinguished from the reconstructed amplitude image. Therefore, the unwrapped phase image was used to analyze the density of living cells. As shown in Fig. 4, the gray distribution of the background in the phase image was not uniform. Furthermore, the phase image was significantly influenced by the white

**Table 1. Time Cost for the Analysis Process of the Cell Culture**

Analysis Process	Data Size (pixels)	Time Cost (s)
Image Collection	$4016 \times 2672$	0.23
Acquisition of the Complex Amplitude Image	$2672 \times 2672$	2.42
Acquisition of the Wrapped Phase Image after Aberration Correction	$390 \times 390$	0.03
Acquisition of the Unwrapped Phase Image	$390 \times 390$	0.35
Image Binarization	$390 \times 390$	0.27
Whole Analysis Process	×	3.30

noises, especially shot noises, which may be caused by the CCD noises or the reflected noises of optical components. Based on the analysis of the image feature, the cell image was segmented as follows: the shot noises were reduced by the median filter with  $5 \times 5$  (pixels), and the image was then enhanced by the Sobel operator with  $3 \times 3$  (pixels). Subsequently, aiming the uneven background, an adaptive threshold algorithm was adopted to transfer the gray image to a binary image. Considering that living cell is generally bigger than the discrete noises, the connection area of a cell is therefore larger than that of noises. Based on this idea, the residual discrete noises can be mostly removed by detecting the pixel number of the connection area. The segmenting result for the unwrapped phase image in Fig. 4 is illustrated in Fig. 5, where living cells are white and the background appears dark. As can be seen, the cell morphology is well segmented, and the total number of white pixels can be easily obtained. The evaluation of the level of confluency was about 11.96% for the TZMbl sample, indicating that there is enough space for cell growth and that cell passage should be done after some time.

The time consumption of the proposed monitoring method for living cell culture was analyzed to evaluate the system performance quantitatively. The program was carried out on a desktop computer with Intel Core 2 Quad 2.66 GHz CPU and 3 GB RAM. For the LFTDH configuration, the numerical reconstruction can be realized by a single inverse fast Fourier transform. Although the image size is  $2672 \times 2672$  (pixels), the time cost for the reconstruction of the complex amplitude image was only 2.42 s. The reconstructed image includes three parts: the zero-order image, the real image, and the virtual image. Only the real image is the region of interest, thus the size of data can be cut into  $390 \times 390$  (pixels) and the processing speed was accelerated, as listed in Table 1. Therefore, the time cost of the whole analysis process for cell culture was about 3.30 s. The two holograms recorded with and without the test sample should be generally acquired in the aberration correction using the two-step phase subtraction method. Furthermore, it is sufficient to record one reference hologram prior the measurement procedure to compensate the phase aberration, ensuring that the status of the cell culture can be observed continuously.

In conclusion, a simple cell imaging method based on digital holography is presented, and the corresponding image post-processing is combined to perform automatic evaluation for the status of cell culture. The LFTDH configuration is developed to collect the hologram of the living cell without prestaining, and the reconstructed amplitude image is acquired by a single fast Fourier transform. The phase aberration is corrected using the two-step phase subtraction method, and the unwrapped

phase image is then obtained by the least-squares phase-unwrapping algorithm. In the imaging experiment of cervical cancer cell TZMbl, the quantitative amplitude and phase information have been retrieved from the digital hologram, and the level of confluency is calculated automatically through the image segmentation of the phase information. The presented method can provide an automatic and non-invasive alternative for monitoring living cell culture.

This work was supported by the National Natural Science Foundation of China (No. 61077004), the Science Foundation of Education Commission of Beijing (No. KZ200910005001), and the Innovative Talent and Team Development for Serving Beijing.

## References

1. J.-S. Kim, L. He, and J. J. Lemasters, *Biochem. Biophys. Res. Commun.* **304**, 463 (2003).
2. M. Onodera, Y. Takikawa, K. Kakisaka, T. Wang, and S. Horiuchi, *Hepatology Research* **40**, 605 (2010).
3. H. Paulenz, IS. Grevle, A. Tverdal, PO. Hofmo, and K. A. Berg, *Reprod. Dom. Anim.* **30**, 107 (1995).
4. Y.-W. Eom, M. A. Kim, S. S. Park, M. J. Goo, H. J. Kwon, S. Sohn, W.-H. Kim, G. Yoon, and K. S. Choi, *Oncogene* **24**, 4765 (2005).
5. N. Lue, W. Choi, G. Popescu, T. Ikeda, R. R. Dasari, K. Badizadegan, and M. S. Feld, *Appl. Opt.* **46**, 1836 (2007).
6. T. Ikeda, G. Popescu, R. R. Dasari, and M. S. Feld, *Opt. Lett.* **30**, 1165 (2005).
7. G. Popescu, T. Ikeda, R. R. Dasari, and M. S. Feld, *Opt. Lett.* **31**, 775 (2006).
8. I. Yamaguchi, *Chin. Opt. Lett.* **7**, 1104 (2009).
9. Y. Zhang, J. Zhao, Q. Fan, and S. Yang, *Chinese J. Lasers (in Chinese)* **37**, 1602 (2010).
10. B. Rappaz, P. Marquet, E. Cuche, Y. Emery, C. Depeursinge, and P. J. Magistretti, *Opt. Express* **13**, 9361 (2005).
11. F. Charrière, N. Pavillon, T. Colomb, C. Depeursinge, T. J. Heger, E. A. D. Mitchell, P. Marquet, and B. Rappaz, *Opt. Express* **14**, 7005 (2006).
12. B. Kemper, D. Carl, J. Schneckenger, I. Bredebusch, M. Schäfer, W. Domschke, and G. von Bally, *J. Biomed. Opt.* **11**, 034005 (2006).
13. A. Mölder, M. Sebesta, M. Gustafsson, L. Gisselsson, A. Gjörlöf-Wingren, and K. Alm, *J. Microsc.* **232**, 240 (2008).
14. C. Yuan, H. Zhai, X. Wang, and L. Wu, *Opt. Commun.* **270**, 176 (2007).
15. P. Ferraro, S. De Nicola, A. Finizio, G. Coppola, S. Grilli, C. Magro, and G. Pierattini, *Appl. Opt.* **42**, 1938 (2003).
16. J. A. Quiroga and E. Bernabeu, *Appl. Opt.* **33**, 6725 (1994).